Universal Frequency-Domain Analysis of N-Path Networks

Mykhailo Tymchenko[®], Aravind Nagulu[®], *Member, IEEE*, Harish Krishnaswamy[®], *Senior Member, IEEE*, and Andrea Alù[®], *Fellow, IEEE*

Abstract—N-path commutated capacitive networks provide a practical solution to implement highly sought on-chip high-Q filtering applications in which the use of lumped inductors is undesirable due to their significant footprints and low Q-factors. Recently, it has been also revealed that N-path networks can also exhibit other interesting functionalities, such as nonreciprocal phase-shifting and ultra-wideband true time delay, providing a path to miniaturization of various reciprocal and nonreciprocal devices. The analytical treatment of these networks, however, remains challenging, because their operation involves frequency mixing produced by the time modulation. In this article, we present a highly accurate frequency-domain approach for the analysis of N-path networks based on perturbation theory. Our method compares favorably to the state-of-the-art polyphase analysis by being much simpler mathematically, yet providing results essentially indistinguishable from numerical simulations, while offering physical insights into the N-path filter operation. We particularize the solution for the high-Q operation regime and obtain simple closed-form analytical expressions for harmonic transfer functions, scattering parameters and baseband impedance.

Index Terms—Switched circuits, circuit analysis, band-pass filters, perturbation methods.

I. Introduction

DUE to the rapid development of various wireless telecommunication technologies, the frequency spectrum has become extremely crowded. The exponential growth of the number of wireless devices has fueled a dramatic increase in demand for data bandwidth, enhancing the problem of interference of neighboring radios. To enable large data bandwidths and reduce interference, all connectivity standards divide their bands into several closely spaced channels, which require

Manuscript received August 2, 2020; revised October 29, 2020 and November 11, 2020; accepted November 12, 2020. Date of publication December 7, 2020; date of current version January 12, 2021. This work was supported in part by the Air Force Office of Scientific Research MURI Program, in part by the Department of Defense Vannevar Bush Faculty Fellowship, in part by the National Science Foundation EFRI Program, and in part by the Simons Foundation. This article was recommended by Associate Editor R. Rieger. (Corresponding author: Andrea Alû.)

Mykhailo Tymchenko was with the Department of Electrical and Computer Engineering, The University of Texas at Austin, Austin, TX 78731 USA. He is now with Lightmatter Inc., Boston, MA 02109 USA.

Aravind Nagulu and Harish Krishnaswamy are with the Department of Electrical Engineering, Columbia University, New York, NY 10027 USA.

Andrea Alù is with the Photonics Initiative, Advanced Science Research Center, The City University of New York, New York, NY 10031 USA, also with the Physics Program, Graduate Center, The City University of New York, New York, NY 10016 USA, and also with the Department of Electrical and Computer Engineering, The University of Texas at Austin, Austin, TX 78712 USA (e-mail: aalu@gc.cuny.edu).

Color versions of one or more figures in this article are available at https://doi.org/10.1109/TCSI.2020.3040592.

Digital Object Identifier 10.1109/TCSI.2020.3040592

high-Q filtering to suppress the crosstalk between channels. To operate under such stringent requirements, modern filters must be software-controlled, provide strong blockage of other channels and be sufficiently compact to fit into the very limited space of modern circuit boards. Traditional high-Q filtering approaches, such as resonant LC circuits and surface/bulk acoustic waves (SAW/BAW) filters, have fundamental limitations that do not allow them to meet these requirements. Stand-alone inductors, in particular, are bulky components that increase footprint and fabrication costs. Monolithic integration of large inductances on a CMOS chip is often impractical due to their extremely large footprints and high loss. SAW/BAW filters, on the other hand, provide excellent linearity and outof-band blocking, but they are not dynamically reconfigurable and are incompatible with CMOS technology. Multiple LC, SAW or BAW filters can be employed in conjunction with a switch network to support reconfigurability, but this comes at the cost of increased insertion loss, footprint and cost, and is ultimately limited by the parasitics seen when multiple switches are connected to a common point.

In view of these challenges, *N*-path filters (or comb filters), originally proposed in 1950s [1]–[3], have resurfaced as a practical solution addressing all the above challenges: they exhibit excellent frequency selectivity, linearity and out-of-band isolation, they are dynamically reconfigurable, and they do not require inductors, making them fully compatible with CMOS technology. A conventional *N*-path filter is shown in Fig. 1(a). It is formed by *N* parallel branches, each containing a shunt capacitance connected to input and/or output ports through a switch. The input and output sets of switches are operated in a sequential non-overlapping fashion with a time delay [see Fig. 1(b)], so that at any instant in time only one branch is connected to each port.

A typical transmission spectrum of such an *N*-path capacitive network consists of multiple narrow peaks located at integer multiples of the switch modulation frequencies. While the first *N*-path networks were switched using mechanical commutators operating at kHz frequencies (thus, the name commutated networks), modern *N*-path filters employ electronic switches implemented using CMOS transistors which are extremely compact and highly linear devices that can operate at GHz frequencies [4]. Despite the fact that *N*-path networks and their key performance metrics, such as bandwidth, insertion and return loss, have been known for almost 60 years, their rigorous theoretical analysis still remains challenging. This is because *N*-path filters employ many switches (i.e., frequency-mixers) modulated by square-wave

1549-8328 © 2020 IEEE. Personal use is permitted, but republication/redistribution requires IEEE permission. See https://www.ieee.org/publications/rights/index.html for more information.

signals which leads to mixing between an infinite number of harmonics. In addition, the reactive elements in each branch provide a memory effect that prevents this circuit from being treated as a purely discrete-time sampling circuit (although this functionality is still possible for some design parameter values). In fact, sampling and filtering regimes of N-path networks correspond to the two opposite asymptotic limits of the relation between the charge/discharge time constant of the capacitor, $\tau = R_0 C$ (R_0 is the port impedance and C is the capacitance of each branch), and the time over which each switch is closed, $\sigma = T_s/N$, with T_s denoting the switching period and N being the number of paths. The sampling regime is achieved when $\tau \ll \sigma$, and the filtering regime is achieved when $\tau \gg \sigma$. In our previous work [5] we showed that the intermediate regime $au \sim \sigma$ implements an ultrawideband true time delay functionality, which allows for dramatic miniaturization of reciprocal and nonreciprocal devices [6], highly beneficial for numerous applications, including analog cancellation approaches in full-duplex applications [7], [8], true-time-delay-based beamforming [9] and analog equalizers [10]. Finally, commutated N-path networks can also exhibit nonreciprocal phase responses when the input and output sets of switches are operated with an asymmetric time delay leading to interesting opportunities for full-duplex communications [11].

Early approaches to N-path filter analysis relied upon signal processing techniques in the complex frequency domain in order to derive the harmonic transfer function (HTF) of N-path networks in the filtering and sampling regimes [12]. These techniques use the fact that, in the vicinity of transmission peaks, N-path filter operation resembles a sampling circuit that enables its treatment as a discrete-time system to obtain an elegant and useful solution for transmitted voltage given the voltages stored in the capacitors [14]. We note, however, that sampling and filtering functionalities correspond to two opposite asymptotic limits, $\tau \ll \sigma$ and $\tau \gg \sigma$, respectively. Thus, the use of such sample-and-hold approximation in the filtering regime must be treated with caution. Other frequency-domain approaches have been based on analyzing the baseband impedance of N-path networks in the assumption of an infinitely large source [15] or load impedance [16], the derivation of HTFs using conversion matrices [17], and z-space analysis [18], [19]. When the N-path network operates in passive-mixer, sampler or high-Q filter modes it can be accurately analyzed using the adjoint network method [20], [21]. A semi-numerical technique developed recently allows for accelerated frequency-domain simulation of N-path networks containing arbitrary blocks in each branch [22]. Finally, one of the most accurate methods for N-path networks analysis is the polyphase approach based on piece-wise reconstruction of the temporal evolution of the network response and a subsequent Fourier transform [23]–[28]. The polyphase technique provides a general solution valid for all combinations of parameters making it the current state-of-the-art. It also enables the accurate analysis of effect of nonidealities such as the presence of parasitic capacitance on N-path network performance [29]. Its drawback, however, is that it is quite cumbersome and involved, and the final solution is so complicated that it is

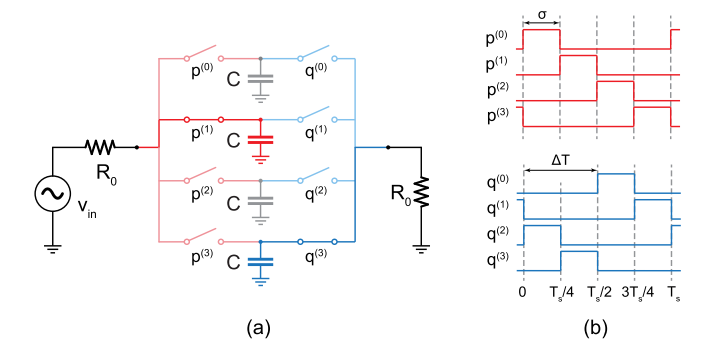


Fig. 1. (a) Schematic of a 4-path 2-port switched capacitor network with source and load impedance R_0 . $p^{(n)}$ and $q^{(n)}$ denote the windowing functions used to model the current flowing through input and output switches, respectively. (b) Profiles of the windowing functions $p^{(n)}(t)$ and $q^{(n)}(t)$ which are 0 when the corresponding switch is open and 1 when it is closed. The switches on each side are operated in a non-overlapping fashion with periodicity T_s . The time over which each switch is closed is $\sigma = T_s/N$, where N is the number of paths (the case of N=4 is displayed). The output set of switches is operated with a delay ΔT with respect to the input set.

often difficult to understand the network's behavior without further analysis. Here, we introduce a simple yet effective approach to frequency-domain analysis of *N*-path capacitive networks based on modified perturbation theory. Compared to the polyphase analysis, our approach yields an equally accurate solution for HTFs and scattering parameters at all frequencies while being much simpler mathematically and offering better insights into the role of all harmonics generated by periodically operated switches in network's operation. In the case when the *N*-path network is operated in the high-Q filtering regime, we derive simple closed-form expressions for HTFs, scattering parameters and baseband impedance in the vicinity of transmission peaks.

II. STATE-SPACE NETWORK ANALYSIS

We consider a 2-port N-path switched capacitor network [the case with N=4 is shown in Fig. 1(a)]. In each branch, labeled $n=0,1,\ldots,N-1$, the switches on either side are operated in revolving fashion with a duty cycle 1/N and a modulation frequency $f_s=1/T_s$. We assume the output switch is delayed with respect to the input switch by a time $\Delta T \in [0,T_s)$ corresponding to a phase shift $\gamma=-2\pi \Delta T/T_s$. In the following we focus on the case of non-overlapping clocks for the input and output switches, but we stress that our analysis remains valid also if the clocks overlap.

We begin by noticing that the current flowing through the capacitor in the n-th branch is equal to the difference between the currents flowing through the input and output switches, as shown in Fig. 2(a):

$$i_c^{(n)}(t) = i_1^{(n)}(t) - i_2^{(n)}(t).$$
 (1)

To model the flow of current through the input and output switches we introduce windowing functions $p^{(n)}(t)$ and $q^{(n)}(t)$,

$$p^{(n)}(t) = \begin{cases} 1, & t \in [-\sigma/2, \sigma/2] + n\sigma, \\ 0, & \text{otherwise,} \end{cases}$$
 (2)

$$q^{(n)}(t) = p^{(n)}(t - \Delta T),$$
 (3)

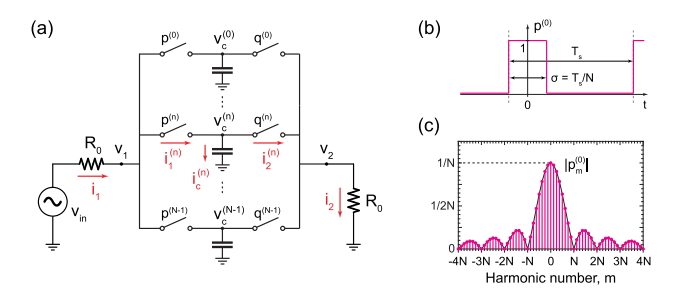


Fig. 2. (a) Schematic of time-varying currents flowing through the n-th branch of the 2-port switched N-path network. (b) Periodic windowing function $p^{(0)}(t)$ of the input switch versus time. The switch is closed when $p^{(0)} = 1$. (c) Fourier spectrum of the switching function $p^{(0)}(t)$ as a function of the harmonics number.

which are 1 when the corresponding switch is closed and 0 at all other times, as shown in Fig. 1(b). $q^{(n)}(t)$ is a replica of $p^{(n)}(t)$ delayed by ΔT . Since we assume that the switch clocks are non-overlapping, we can relate the currents $i_1^{(n)}(t)$ and $i_2^{(n)}(t)$ to the currents flowing through the source and load resistances, $i_1(t)$ and $i_2(t)$, simply as

$$i_1^{(n)}(t) = p^{(n)}(t)i_1(t),$$
 (4)

$$i_2^{(n)}(t) = q^{(n)}(t)i_2(t).$$
 (5)

Combining Eqs. (1)-(5), we obtain

$$i_c^{(n)}(t) = p^{(n)}(t)i_1(t) - q^{(n)}i_2(t).$$
 (6)

Assuming that both ports have the same constant and real impedance R_0 , we apply the Kirchhoff's voltage law to obtain

$$C\frac{dv_c^{(n)}(t)}{dt} = p^{(n)}(t)\frac{v_{in}(t) - v_c^{(n)}(t)}{R_0} - q^{(n)}(t)\frac{v_c^{(n)}(t)}{R_0}, \quad (7)$$

which after rearrangement of terms can be re-written as

$$\left[p^{(n)}(t) + q^{(n)}(t) + \tau \frac{d}{dt}\right] v_c^{(n)}(t) = p^{(n)}(t) v_{in}(t). \tag{8}$$

Eq. (8) is equivalent to the state-space equation (or coupled-mode equation) for a capacitor voltage used in the polyphase analysis [23]–[28]. Periodic windowing functions $p^{(n)}(t)$ and $q^{(n)}(t)$ can be presented as Fourier series

$$\left\{ \begin{array}{l} p^{(n)}(t) \\ q^{(n)}(t) \end{array} \right\} = \sum_{m=-\infty}^{\infty} \left\{ \begin{array}{l} p_m^{(n)} \\ q_m^{(n)} \\ \end{array} \right\} e^{jm\omega_s t}, \tag{9}$$

where m is integer, $\omega_s = 2\pi f_s$ is the angular switching frequency, and $p_m^{(n)}$ and $q_m^{(n)}$ are Fourier coefficients defined

$$\begin{cases} p_m^{(n)} \\ q_m^{(n)} \end{cases} = \frac{1}{T_s} \int_{-T_s/2}^{T_s/2} \begin{cases} p^{(n)}(t) \\ q^{(n)}(t) \end{cases} e^{-jm\omega_s t}. \tag{10}$$

Substituting (2) into (10), for $p_m^{(n)}$ we obtain

$$p_m^{(n)} = e^{jmn\omega_s \sigma} \frac{1}{T_s} \int_{-\sigma/2}^{\sigma/2} e^{-jm\omega_s t} dt = p_m e^{-j\frac{2\pi}{N}mn}, \quad (11)$$

where p_m are harmonics of the windowing function of the n = 0 branch,

$$p_m \equiv p_m^{(0)} = \frac{1}{N} \operatorname{sinc}_{\pi} \left(\frac{m}{N} \right), \tag{12}$$

and $\operatorname{sinc}_{\pi}(x)$ is defined as

$$\operatorname{sinc}_{\pi}(x) = \begin{cases} \frac{\sin(\pi x)}{\pi x}, & x \neq 0, \\ 1, & x = 0. \end{cases}$$
 (13)

The windowing function $p^{(0)}(t)$ and its spectrum $p_m^{(0)}$ are plotted in Fig. 2(b) and 2(c), respectively, with $|p_m^{(0)}| \le$ 1/N for all m. Due to (3), the Fourier harmonics $q_m^{(n)}$ can be obtained from $p_m^{(n)}$ by simply applying the appropriate phase-shift:

$$q_m^{(n)} = p_m^{(n)} e^{-jm\omega_s \Delta T}. \tag{14}$$

The voltage $v_c^{(n)}(t)$ across the capacitor in each branch can be presented as a Floquet state containing a discrete set of harmonics oscillating at angular frequencies $\omega_k = \omega + k\omega_s$ with $\omega = 2\pi f$ and k being integer:

$$v_c^{(n)}(t) = \sum_{k=-\infty}^{\infty} v_{c,k}^{(n)} e^{j\omega_k t} = \sum_{k=-\infty}^{\infty} v_{c,k} e^{-jnk\omega_s \sigma + j\omega_k t}, \quad (15)$$

where $v_{c,k} \equiv v_{c,k}^{(0)}$. Substituting (9) and (15) into (8), assuming that the input voltage is monochromatic, $v_{in}(t) = v_{in}e^{j\omega t}$, and invoking the Cauchy product rule, we obtain the following infinite system of equations for the n = 0 branch:

$$\sum_{k=-\infty}^{\infty} M_{mk} h_{c,k} = p_m, \tag{16}$$

where $h_{c,k} = v_{c,k}/v_{in}$ are HTFs between the fundamental harmonic of the source and k-th harmonic of the capacitor voltage. The matrix elements M_{mk} are given as

$$M_{mk} = U_{mk} + \delta_{m,k} \, i \omega_k \tau, \tag{17}$$

where $\delta_{m,k}$ is the Dirac's delta-function, and U_{mk} is a Toeplitz matrix containing the sum of Fourier coefficients of the windowing functions,

$$U_{mk} \equiv u_{m-k} = p_{m-k} + q_{m-k}, \tag{18}$$

so that $U_{mk}^* = U_{km}$ with the asterisk denoting the complex conjugate. In vector-matrix form, the system (16)-(17) can be recast as

$$\mathbf{M} \cdot \mathbf{h}_c = \mathbf{p},\tag{19}$$

where

$$\mathbf{h}_c = (\dots, h_{c,-1}, h_{c,0}, h_{c,1}, \dots)^T,$$

 $\mathbf{p} = (\dots, p_{-1}, p_0, p_1, \dots)^T,$

with T denoting the transpose, and

bestituting (2) into (10), for
$$p_m^{(n)}$$
 we obtain
$$p_m^{(n)} = e^{jmn\omega_s\sigma} \frac{1}{T_s} \int_{-\sigma/2}^{\sigma/2} e^{-jm\omega_s t} dt = p_m e^{-j\frac{2\pi}{N}mn}, \quad (11)$$

$$\text{ere } p_m \text{ are harmonics of the windowing function of the}$$

$$= 0 \text{ branch,}$$

$$p_m \equiv p_m^{(0)} = \frac{1}{N} \operatorname{sinc}_{\pi} \left(\frac{m}{N}\right), \quad (12)$$

$$M = \begin{bmatrix} \ddots & & \vdots & & \\ u_0 + j\omega_{-1}\tau & u_{-1} & u_{-2} & & \\ u_1 & u_0 + j\omega_{0}\tau & u_{-1} & & \\ u_2 & u_1 & u_0 + j\omega_{1}\tau & & \\ \vdots & & \ddots & \end{bmatrix}.$$

$$(20)$$

In principle, it is straightforward to solve system (19) numerically by computing the inverse of the matrix \mathbf{M} . However, to do so the system needs to be truncated at some harmonic K, which for square-wave modulation results in slow convergence, rapidly growing computation complexity and numerical artifacts. In addition, this approach does not provide much insight into the N-path network operation. Rather than solving this system numerically, in the following we show that we can leverage the peculiar structure of the matrix \mathbf{M} to analytically solve for \mathbf{h}_c .

III. N-PATH CAPACITIVE NETWORK ANALYSIS USING PERTURBATION THEORY

From (12) and (14) we conclude that all terms u_m in the matrix \mathbf{M} in the system (19)-(20) have an upper bound, $|u_m| \leq 2/N$ for all m, with the largest element being $u_0 = p_0 + q_0 = 2/N$. The magnitudes of all off-diagonal elements of the matrix exhibit oscillatory decay as we move away from the main diagonal, owing to interference between the phase-shifted spectra of the windowing functions. By recalling that $\omega_k = \omega + k\omega_s$, we also conclude that the magnitudes of the terms $jk\omega_s\tau$ on the main diagonal grow monotonically with |k|. Thus, for any real $\varepsilon > 0$ there always exists an integer K such that for |k| > K we have $|\omega_k\tau| - u_0 > \varepsilon$. In other words, with increasing $|k + \omega/\omega_s|$ the magnitudes of the terms on the main diagonal grow monotonically, and eventually become much larger than all off-diagonal terms.

The conventional N-path filter operates in the regime when the time-constant of the capacitance in each branch is much larger than the time over which each switch is closed, $\tau \ll \sigma$, or, equivalently, $f_s \tau \ll 1/N$. In this case, *all* elements on the main diagonal of the matrix \mathbf{M} are much larger than all off-diagonal elements except, possibly, one element with frequency $f_r = f + rf_s$ which happens to be near DC, i.e., $f_r \approx 0$. This can occur at $f/f_s = 0, 1, 2, \ldots$ corresponding to $r = 0, -1, -2, \ldots$, respectively. We also notice that when $f_r = 0$ the magnitude of the corresponding element on the diagonal, $M_{rr}(f_r = 0) = 2/N$, is of the same order as the off-diagonal elements. Without this unique element on the main diagonal, we could use a standard perturbation method [30] to analytically compute \mathbf{M}^{-1} and solve the system (19).

Perturbation theory states that the inverse of a matrix $\mathbf{A} + \delta \mathbf{A}$ with \mathbf{A} being a square matrix with a non-degenerate set of eigenvalues and $\delta \mathbf{A}$ being a small perturbation, can be computed to the first-order correction as (see Appendix A)

$$(\mathbf{A} + \delta \mathbf{A})^{-1} \approx \mathbf{A}^{-1} - \mathbf{A}^{-1} \cdot \delta \mathbf{A} \cdot \mathbf{A}^{-1}.$$
 (21)

Here, the fact that the perturbation $\delta \mathbf{A}$ is small should be understood in the sense that it does not significantly perturb the eigenvalues of \mathbf{A} . Eq. (21) is particularly useful when the matrix \mathbf{A} is diagonal, because in this case its inversion is trivial, allowing for analytical computation of $(\mathbf{A} + \delta \mathbf{A})^{-1}$. However, since one of the elements on the main diagonal of the matrix \mathbf{M} is small, we cannot apply (21) right away, as the corresponding eigenvalue may be significantly affected.

To overcome this difficulty, we separate all harmonics in two subsets [31]: a finite subset \mathcal{R} containing a single or multiple

harmonics closest to DC, and an infinite subset \mathcal{N} comprising all other harmonics, $\mathcal{N} = \mathcal{I} \backslash \mathcal{R}$, where \mathcal{I} are all integers. The system (19) can be accordingly split into

$$\begin{cases}
\mathbf{M}_{\{\mathcal{R},\mathcal{R}\}} \cdot \mathbf{h}_{c,\{\mathcal{R}\}} + \mathbf{M}_{\{\mathcal{R},\mathcal{N}\}} \cdot \mathbf{h}_{c,\{\mathcal{N}\}} = \mathbf{p}_{\{\mathcal{R}\}}, \\
\mathbf{M}_{\{\mathcal{N},\mathcal{R}\}} \cdot \mathbf{h}_{c,\{\mathcal{R}\}} + \mathbf{M}_{\{\mathcal{N},\mathcal{N}\}} \cdot \mathbf{h}_{c,\{\mathcal{N}\}} = \mathbf{p}_{\{\mathcal{N}\}},
\end{cases} (22)$$

where the submatrices $\mathbf{M}_{\{\mathcal{R},\mathcal{N}\}}$ and $\mathbf{M}_{\{\mathcal{N},\mathcal{R}\}}$ contain elements M_{ml} with $m \in \mathcal{R}, l \in \mathcal{N}$ and $m \in \mathcal{N}, l \in \mathcal{R}$, respectively. In turn, indices of the square submatrices $\mathbf{M}_{\{\mathcal{R},\mathcal{R}\}}$ and $\mathbf{M}_{\{\mathcal{N},\mathcal{N}\}}$, and vectors $\mathbf{h}_{c,\{\mathcal{R}\}}$ and $\mathbf{h}_{c,\{\mathcal{N}\}}$, span over the subsets \mathcal{R} and \mathcal{N} , correspondingly. We also note that for the two off-diagonal submatrices we have $\mathbf{M}_{\{\mathcal{R},\mathcal{N}\}} \equiv \mathbf{U}_{\{\mathcal{R},\mathcal{N}\}}$ and $\mathbf{M}_{\{\mathcal{N},\mathcal{R}\}} \equiv \mathbf{U}_{\{\mathcal{N},\mathcal{R}\}}$, which yields

$$\begin{cases}
\mathbf{M}_{\{\mathcal{R},\mathcal{R}\}} \cdot \mathbf{h}_{c,\{\mathcal{R}\}} + \mathbf{U}_{\{\mathcal{R},\mathcal{N}\}} \cdot \mathbf{h}_{c,\{\mathcal{N}\}} = \mathbf{p}_{\{\mathcal{R}\}}, \\
\mathbf{U}_{\{\mathcal{N},\mathcal{R}\}} \cdot \mathbf{h}_{c,\{\mathcal{R}\}} + \mathbf{M}_{\{\mathcal{N},\mathcal{N}\}} \cdot \mathbf{h}_{c,\{\mathcal{N}\}} = \mathbf{p}_{\{\mathcal{N}\}}.
\end{cases} (23)$$

Since the submatrix $\mathbf{M}_{\{\mathcal{N},\mathcal{N}\}}$ is square and *all* its elements on the main diagonal are much larger than the off-diagonal elements, we can analytically compute $\mathbf{M}_{\{\mathcal{N},\mathcal{N}\}}^{-1}$ using (21) and obtain the solution for $\mathbf{h}_{c,\{\mathcal{N}\}}$ as a function of $\mathbf{h}_{c,\{\mathcal{R}\}}$:

$$\mathbf{h}_{c,\{\mathcal{N}\}} = \mathbf{M}_{\{\mathcal{N},\mathcal{N}\}}^{-1} \cdot \left[\mathbf{p}_{\{\mathcal{N}\}} - \mathbf{U}_{\{\mathcal{N},\mathcal{R}\}} \cdot \mathbf{h}_{c,\{\mathcal{R}\}} \right]. \tag{24}$$

To compute the inverse of the matrix $M_{\{\mathcal{N},\mathcal{N}\}}$, we separate its main diagonal from the rest of the matrix:

$$\left[\mathbf{M}_{\{\mathcal{N},\mathcal{N}\}}\right]_{m,l} = \delta_{m,l}d_l + (1 - \delta_{m,l})u_{m-l}, \quad m, l \in \mathcal{N}, \quad (25)$$

with d_l denoting the elements on the main diagonal:

$$d_l = u_0 + j\omega_l \tau, \tag{26}$$

such that $|d_l| \gg u_0$ for all $l \in \mathcal{N}$. Using Eq. (21), we obtain

$$\left[\mathbf{M}_{\{\mathcal{N},\mathcal{N}\}}^{-1}\right]_{l,m} \approx \delta_{l,m} \frac{1}{d_l} - (1 - \delta_{l,m}) \frac{u_{l-m}}{d_l d_m}, \quad l, m \in \mathcal{N}. (27)$$

Substituting (27) into (24), we obtain the solution for $\mathbf{h}_{c,\{\mathcal{N}\}}$:

$$h_{c,l} = \frac{1}{d_l} \left(\tilde{p}_l - \sum_{r \in \mathcal{R}} u_{l-r} h_{c,r}, \right), \quad l \in \mathcal{N},$$
 (28)

where \tilde{p}_l plays the same role as p_l but re-normalized to account for second-order scattering via all other harmonics in the subset \mathcal{N} :

$$\tilde{p}_k = p_k - \sum_{m \in \mathcal{N}} (1 - \delta_{k,m}) \frac{u_{k-m} p_m}{d_m},$$
 (29)

where k can be any integer. From Eq. (28), it is seen that the first term corresponds to the contribution of linear and second-order scattering of the incoming voltage through all windowing function harmonics in the subset \mathcal{N} , while the second term corresponds to re-scattering of voltage harmonics in the subset \mathcal{R} to the l-th harmonic. In the latter we retained only terms linear in u_{l-r} , because they already correspond to second-order scattering of the input voltage through all harmonics in the subset \mathcal{R} .

Substituting Eq. (24) into the first equation of (22), we obtain the following system of equations for $\mathbf{h}_{c,\{\mathcal{R}\}}$ only:

$$\sum_{q \in \mathcal{R}} \tilde{M}_{rq} h_{c,q} = \tilde{p}_r, \quad r \in \mathcal{R}, \tag{30}$$

where \tilde{p}_r is given by Eq. (29), and the matrix elements \tilde{M}_{rq} are

$$\tilde{M}_{rq} = \tilde{U}_{rq} + \delta_{r,q} j \omega_q \tau, \quad r, q \in \mathcal{R},$$
 (31)

with \tilde{U}_{rq} playing the same role as $U_{rq} \equiv u_{r-q}$ but re-normalized to account for second-order scattering through all harmonics in the subset \mathcal{N} :

$$\tilde{U}_{rq} = u_{r-q} - \sum_{m \in \mathcal{N}} \frac{u_{r-m} u_{m-q}}{d_m}.$$
 (32)

The new system (30) and the initial system (16) have identical structures, but the new system is *finite*, i.e., quite remarkably, we managed to reduce the system describing the commutated network, with an infinite number of equations, to the finite linear system (30) for voltage harmonics in the subset \mathcal{R} , which can be solved *in closed form* without running into convergence issues. In other words, we replaced the inversion of the originally infinite matrix \mathbf{M} and associated computational problems with the inversion of a small matrix $\tilde{\mathbf{M}}_{\{\mathcal{R},\mathcal{R}\}}$ defined in Eq. (31) and a few simple summations over windowing function harmonics that are numerically very cheap. The parameters determining the convergence of the solution are the size of the subsets \mathcal{R} and \mathcal{N} , which depend on the specific operation of the N-path device.

The output voltage $v_2(t)$ across the load can be found as

$$v_2(t) = \sum_{n=0}^{N-1} q^{(n)}(t) v_c^{(n)}(t), \tag{33}$$

which after the Fourier transform becomes

$$v_{2,k} = \sum_{m=-\infty}^{\infty} \sum_{n=0}^{N-1} q_{k-m}^{(n)} v_{c,m}^{(n)}$$

$$= \sum_{m=-\infty}^{\infty} \sum_{n=0}^{N-1} q_{k-m} e^{-j\omega_s(k-m)n\sigma} v_{c,m} e^{-j\omega_s mn\sigma}$$

$$= \left[\sum_{n=0}^{N-1} e^{-j\omega_s kn\sigma} \right] \sum_{m=-\infty}^{\infty} q_{k-m} h_{c,m} v_{in}, \quad k \in \mathcal{I}. \quad (34)$$

The summation in the square brackets can be performed explicitly:

$$\sum_{n=0}^{N-1} e^{-j\omega_s kn\sigma} = N\delta_{k,sN}, \quad k, s \in \mathcal{N},$$
 (35)

so that we obtain

$$v_{2,k} = N\delta_{k,sN} \sum_{m=-\infty}^{\infty} q_{sN-m} h_{c,m} v_{in}$$

$$= N\delta_{k,sN} \sum_{m=-\infty}^{\infty} p_{sN-m} e^{-j(sN-m)\omega_s \Delta T} h_{c,m} v_{in}, \ k, s \in \mathcal{I}.$$
(36)

From Eq. (36) it follows that the only non-zero harmonics at input and output ports are those with $k = 0, \pm N, \pm 2N, ...$, in agreement with the operation of N-path filters. The corresponding HTF between input voltage and the k-th harmonic of v_2 across the load, $h_{21,k} = v_{2,k}/v_{in}$, is found to be

$$h_{21,k} = N\delta_{k,sN} \sum_{m=-\infty}^{\infty} p_{sN-m} e^{-j(sN-m)\omega_s \Delta T} h_{c,m}, \quad k, s \in \mathcal{I}.$$
(37)

By analogy with (33), we can also find the voltage v_1 ,

$$v_1(t) = \sum_{n=0}^{N-1} p^{(n)}(t) v_c^{(n)}(t), \tag{38}$$

which, following the same procedure, yields

$$h_{11,k} = N\delta_{k,sN} \sum_{m=-\infty}^{\infty} p_{sN-m} h_{c,m}, \quad k, s \in \mathcal{I}.$$
 (39)

Finally, the Floquet scattering parameter $S_{ij,mn}$ that relates the amplitudes of the m^{th} harmonic of the power wave exiting from port i to the amplitude of the n^{th} harmonic of the power wave entering port j (see Appendix B) can be computed from the corresponding HTF as (see Appendix C)

$$S_{ij,mn} = 2h_{ij,mn} - \delta_{ij}\delta_{mn}, \tag{40}$$

where $h_{ij,mn} \equiv h_{ij,m-n}$.

A. Summary of the Solution Procedure

To help the reader navigate the solution flow, here we briefly outline all required steps to obtain a complete and accurate solution for all HTFs and scattering parameters of a 2-port *N*-path network.

1) Given the switching functions $p^{(0)}(t)$ and $q^{(0)}(t)$, compute Fourier spectra p_m and q_m , and their sum $u_m = p_m + q_m$. This step needs to be performed once and the obtained Fourier spectra are valid for all frequencies.

Next, for every angular frequency ω :

- 2) Find integer $r_0 < 0$ for which $\omega + r_0\omega_s$ is closest to zero. The choice of r_0 affects which harmonics will be included in the subset \mathcal{R} and treated separately from all other harmonics.
- 3) Choose the subset \mathcal{R} such that it is centered at r_0 and includes multiple harmonics around it, e.g. $\mathcal{R} = \{r_0 15, \dots, r_0, \dots, r_0 + 15\}$. Then chose the maximum harmonic number M and obtain the subset $\mathcal{N} = \mathcal{I} \setminus \mathcal{R}$ where \mathcal{I} is all integers, in this case $\mathcal{N} = \{-M, \dots, r_0 16, r_0 + 16, \dots, M\}$.
- 4) Compute d_m using Eq. (26).
- 5) Compute \tilde{p}_k and \tilde{U}_{rq} using Eqs. (29) and (32), respectively.
- 6) Using Eq. (30), compute the finite submatrix $\tilde{\mathbf{M}}_{\{\mathcal{R},\mathcal{R}\}}$ and its inverse $\mathbf{F} = \tilde{\mathbf{M}}_{\{\mathcal{R},\mathcal{R}\}}^{-1}$. If the subset \mathcal{R} contains only one harmonic r_0 , the matrix \mathbf{F} is reduced to a single element.
- 7) Compute capacitor voltage HTFs $h_{c,r}$ in the subset \mathcal{R} :

$$h_{c,r} = \sum_{q \in \mathcal{R}} F_{rq} \tilde{p}_q, \quad r \in \mathcal{R}.$$

¹The procedure of elimination of a subset of unknown variables in a system of equations and solving only for remaining unknowns is called *Kron reduction* [32], which is an ubiquitous technique in classic circuit and graph theory. Here, we use this technique to eliminate all harmonics in the infinite subset \mathcal{N} and initially solve only for harmonics in the finite subset \mathcal{R} .

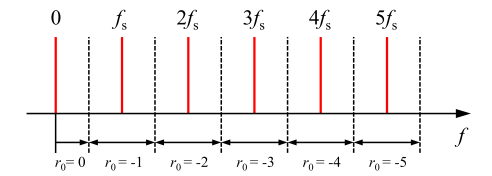


Fig. 3. To obtain the solution over the entire frequency range, we split the latter into intervals separated by dashed vertical lines. Each interval is centered around $-r_0 f_s$ with $r_0 = 0, -1, -2, \ldots$ being the only harmonics in the subset \mathcal{R} . The first interval is truncated to include only positive frequencies. The final solution is obtained by stitching together solutions in each interval.

- 8) Using Eq. (27), compute remaining capacitor voltage HTFs $h_{c,l}$ with $l \in \mathcal{N}$.
- 9) Compute HTFs for input and output voltages, $h_{11,k}$ and $h_{21,k}$, using Eqs. (39) and (37), respectively. To obtain $h_{12,k}$ and $h_{22,k}$ we can simply swap windowing function harmonics p_m and q_m everywhere.
- 10) Compute Floquet scattering parameters using Eq. (40). If the obtained solution contains abrupt discontinuities, one should increase the number of harmonics in the subset \mathcal{R} (and, possibly, in \mathcal{N}) and repeat steps 2-10.

IV. COMPARISON WITH NUMERIC SIMULATIONS

The accuracy of the analytical solution developed in the previous section relies on the particular choice of the subset \mathcal{R} and the number of harmonics in the subset \mathcal{N} . Since the choice of \mathcal{R} depends on f and f_s , it needs to be revised as the operation frequency is swept across the spectrum. For each frequency f, the best choice of \mathcal{R} is the one centered around $r_0 = -k$ for which f is the closest to kf_s with k = $0, 1, 2, \ldots$, as shown in Fig. 3. In addition, \mathcal{R} must also include all harmonics around r_0 , i.e., $\{r_0-m,\ldots,r_0,\ldots,r_0+m\}$ with m being a positive integer, for which the condition $|f+mf_s| \gg$ $1/N\tau$ is not fulfilled. As a result of this procedure, in each frequency interval in Fig. 3, we obtain a separate solution curve with highest accuracy at $f = kf_0$ that becomes less accurate as we approach the edge of the interval. For such a piece-wise solution, we may incur nonphysical discontinuities at the borders between these intervals. To overcome this issue and remove discontinuities, we can increase the number of harmonics included in until all artifacts disappear.

In Fig. 4(a, b), we plot the amplitude and phase of the calculated scattering parameters for an 8-path commutated network with a shunt capacitance C=10 pF in each branch switched at $f_s=1$ GHz with a commutation phase shift $\Delta T=T_s/2$. In this case the phase response of the network is symmetric, hence reciprocal at all frequencies. Since for such a network $\tau\gg\sigma$, it is sufficient to include only one harmonic r_0 in \mathcal{R} . We also choose $\mathcal{N}=\{-60,\ldots,r_0-1,r_0+1,\ldots,+60\}$. It is seen that over the entire frequency range of interest the analytical results agree very well with simulations performed using the Periodic Steady State (PSS) solver of Cadence SpectreRF [33] while being computationally much cheaper.² Another important advantage of our approach is the

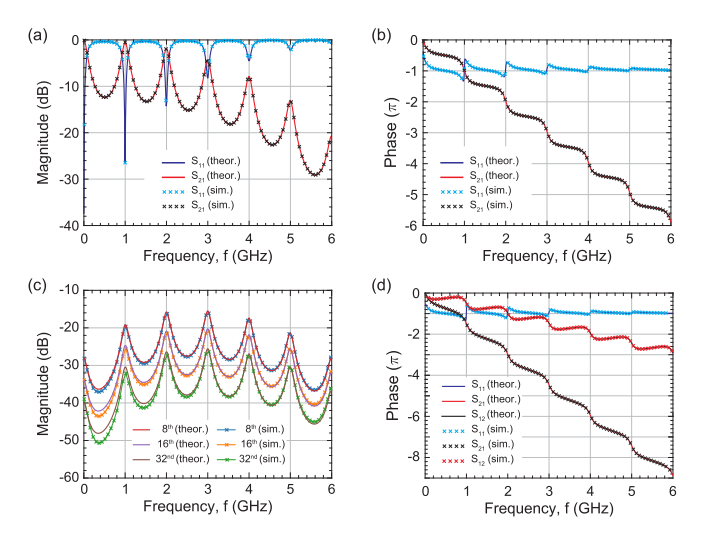


Fig. 4. Magnitude (a) and phase (b) of scattering parameters of an 8-path switched capacitor network with $f_S=1$ GHz, $R_0=50$ ohm and C=10 pF corresponding to the high-Q filtering regime. Analytic curves are plotted with solid lines; markers indicate numerical results obtained using the PSS solver [33]. The output set of switches is delayed with respect to the input set by a time period $\Delta T=T_S/2$ in which case the network response is fully reciprocal, $S_{21}=S_{12}$. (c) Simulated and analytically computed first three non-zero harmonics of S_{21} (8th, 16th and 32nd). (d) Phase of scattering parameters for $\Delta T=3T_S/4$ in which case the network exhibits a phase-nonreciprocal response. The magnitudes of the scattering parameters are the same as in panel (a).

fact that it can easily handle an arbitrary number of paths, while numerical simulations require setting up a new circuit if the number of paths is modified, which can be quite time-consuming. This feature makes the theoretical solution quite valuable for rapid prototyping.

In Fig. 4(c), we also compare the first three non-zero harmonics of S_{21} (for an 8-path network these are 8^{th} , 16^{th} and 32^{nd} harmonics). Once again, we find excellent agreement between theoretical and numerical curves, except at frequencies below 1 GHz where they differ slightly. We argue, however, that the theoretically computed curves are more accurate because the solution is frequency-independent, while the time-domain simulations tend to yield less accurate results at low frequencies due to prolonged simulation times required to obtain an accurate spectral response. Finally, in Fig. 4(d) we show the theoretically and numerically computed phases of S_{21} and S_{12} for $\Delta T = 3T_s/4$, leading to a nonreciprocal phase response, which has recently enabled the realization of a magnetless circulator [11]. The magnitudes of the corresponding scattering parameters in this case are the same as in Fig. 4(a).

We may now consider the same network but with C=1.4 pF, corresponding to $\tau \sim \sigma$. In this regime the N-path network operates as a broadband true-time delay [5], hence we can expect more harmonics to enter into the analysis. To obtain high solution accuracy and avoid nonphysical jumps at intervals' edges we need to include more harmonics to the subset \mathcal{R} . We choose $\mathcal{R} = \{r_0 - 15, ..., r_0 - 1, r_0, r_0 + 1, ..., r_0 + 15\}$ and all remaining harmonics are included in $\mathcal{N} = \{-60, ..., +60\} \setminus \mathcal{R}$. The resulting magnitudes and phases of the scattering parameters computed using our approach and Cadence SpectreRF for $\Delta T = T_s/2$ are plotted

²Typical computation times for an 8-path network time-domain simulation performed in Cadence SpectreRF running on a dedicated server are between 1 and 2 minutes. All analytic results presented in this article were computed using a Python code [34] running on a laptop with modest specifications and took about 20 seconds for the same number of frequency points.

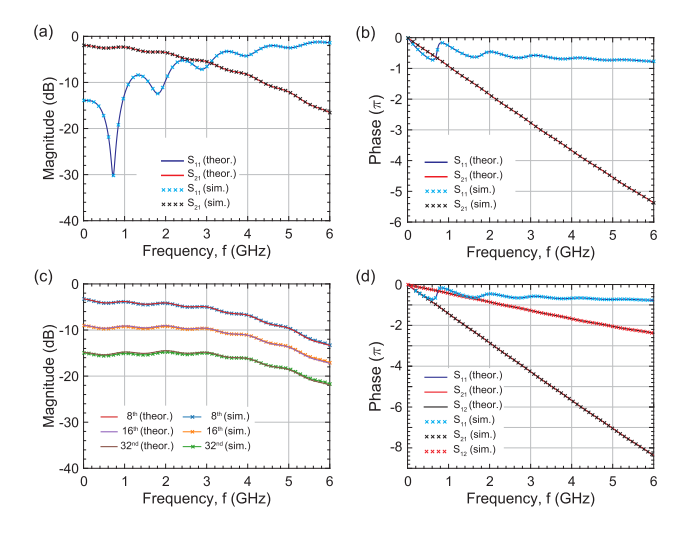


Fig. 5. Same as Fig. 4 but for C = 1.4 pF corresponding to the ultrawideband transmission regime with linear phases of S_{21} and S_{12} over the entire transmission band.

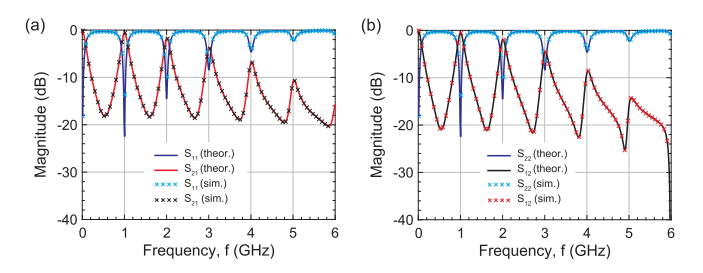


Fig. 6. Analytical (solid lines) and simulated (markers) scattering parameters of an 8-path switched capacitor network with C=10 pF, $R_0=50$ ohm, $f_s=1$ GHz, and overlapping clocks of input and output sets of switches. Switches at port 2 lag switches at port 1 by $\Delta T=T_s/32$, i.e. clock signals have 75% overlap. Panels (a) and (b) correspond to network being excited from port 1 and 2, respectively.

in Fig. 5(a, b). It is seen that for the chosen parameters all results showcase excellent agreement at all frequencies. The theoretical curves in Fig. 5 took slightly longer to compute, yet still much faster than numerical simulations, compared to those in Fig. 4, since in this case we have to invert a 31×31 matrix at each frequency.

Finally, it is instructive to compare analytical and numerical solutions in the case when the windowing functions $p^{(n)}(t)$ and $q^{(n)}(t)$ overlap. Indeed, the original KCL equation (6) for the node in n-th branch does not prohibit the overlap, and thus the solution developed in Section III is expected to remain valid also for the case of overlapping clocks. Here we stress that by overlapping clocks we mean clocks of input and output switches *on the same branch*. The clocks of different paths still must be non-overlapping.

In Fig. 6 we plot the magnitude of S-parameters of an N-path network for $\Delta T = T_s/32$, i.e., output clocks have 75% overlap with input clocks. Once again we observe excellent agreement between results obtained by means of our method and Cadence simulations. Note that when input and output clocks overlap, the network becomes nonreciprocal ($S_{21} \neq S_{12}$), owing to the fact that the order in which input and output switches are closed is different for signals entering

from port 1 and port 2. For signals entering through port 1, the input switch is closed before the output one. In turn, for signals entering from port 2, the output switch is closed before the input switch. As a result, the average amount of energy stored in the capacitors will differ slightly, leading to nonreciprocal transmission.

V. ANALYTIC SOLUTION FOR THE N-PATH FILTER

As we saw in the previous Section, when the N-path network is in the filtering regime, $\tau\gg\sigma$, it is sufficient to include only one harmonic in the subset \mathcal{R} . In this Section, we leverage this property to obtain closed-form expressions for the scattering parameters of an N-path network operating as a high-Q filter in the vicinity of its transmission peaks. Since $\tau\gg\sigma$, all elements d_k on the main diagonal of the matrix \mathbf{M} are large, excluding one element $d_r=u_0+j\omega_r\tau$ with $\omega_r=\omega+r\omega_s\approx0$ (r is negative integer). This condition is achieved when $f\approx-rf_s$. Separating this special harmonic from the rest, we obtain that $\mathcal{R}=\{r\}$ and $\mathcal{N}=\mathcal{I}\backslash\mathcal{R}$. Since the subset \mathcal{R} contains only a single index r, from Eq. (30) we obtain the following equation for the corresponding HTF for the capacitor voltage $h_{c,r}$

$$(\tilde{U}_{rr} + j\omega_r \tau)h_{c,r} = \tilde{p}_r, \tag{41}$$

which yields

$$h_{c,r} = \frac{\tilde{p}_r}{\tilde{U}_{rr} + j\omega_r \tau} \approx \frac{p_r}{u_0 + j\omega_r \tau} = \frac{p_r}{d_r},\tag{42}$$

with the denominator $d_r = u_0 + j\omega_r\tau$ containing a pole $\omega_r^{\rm pole} = -r\omega_s + ju_0/\tau$ (remember that $r \leq 0$) in the complex angular frequency plane. Thus, it becomes clear that $h_{c,r} = v_{c,r}/v_{in}$ reaches its maximum when $\omega = \mathrm{Re}\,\omega_r^{\mathrm{pole}}$, i.e., when the input monochromatic signal is in resonance (i.e., synchronized) with the r-th harmonic of the windowing function, p_r , oscillating at $|r|\omega_s$. The width of the resonance depends on $u_0/\tau = 2/N\tau$ from which we can intuitively understand the fact that the increase in the number of paths or the time constant τ leads to a narrower transmission window: the pole moves closer to the real axis leading to a higher Q-factor.

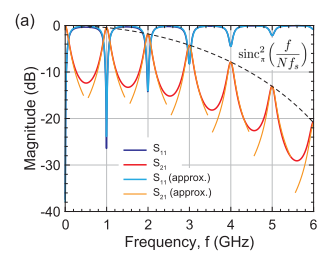
Next, since $|d_l| \gg u_k$ for any $l \in \mathcal{N}$ and any k, we can also simplify the solution (28) for $h_{c,l}$:

$$h_{c,l} \approx \frac{1}{d_l} \left(p_l - \frac{u_{l-r} p_r}{d_r} \right), \quad l \in \mathcal{N},$$
 (43)

where we used the fact that $\tilde{p}_l \approx p_l$. For $\omega_r = 0$ (i.e. when $\omega = -r\omega_s$), we have $d_r = u_0$, but $|d_l|$ is still much larger than $|u_k|$ for any k. Thus, we conclude that $|h_{c,l}| \ll |h_{c,r}|$ for all $l \in \mathcal{N}$, and summations in (37) and (39) reduce to a single term:

$$h_{21,k} \approx N \delta_{k,sN} \frac{p_{sN-r} p_r}{d_r} e^{-j(sN-r)\omega_s \Delta T}, \tag{44}$$

$$h_{11,k} \approx N\delta_{k,sN} \frac{p_{sN-r}p_r}{d_r}, \quad k,s \in \mathcal{I}.$$
 (45)



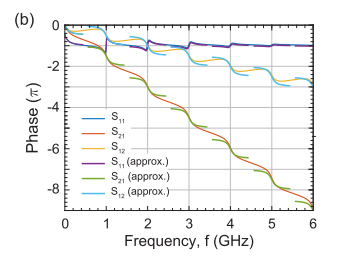


Fig. 7. Magnitude (a) and phase (b) of the scattering parameters of an 8-path switched capacitor network operated at $f_s=1$ GHz, $R_0=50$ ohm, C=10 pF (filtering regime) and $\Delta T=3T_s/4$. Simplified analytic solutions obtained in the vicinity of $f=0,\,f_s,2f_s,\ldots$ by means of Eqs. (50) and (51) are plotted versus full analytic solution of Eqs. (37), (39) and (40).

For the fundamental harmonic, these expressions can be further simplified to

$$h_{21,0} \approx N \frac{p_{-r} p_r}{d_r} e^{jr\omega_s \Delta T} = \frac{\operatorname{sinc}_{\pi}^2 (r/N)}{2 + j\omega_r N \tau} e^{jr\omega_s \Delta T}, \quad (46)$$

$$h_{11,0} \approx \frac{\mathrm{sinc}_{\pi}^2(r/N)}{2 + i\omega_r N\tau}.$$
 (47)

The above expressions reveal that the response of the N-path filter at the fundamental frequency in the vicinity of m-th transmission peak is due to resonant excitation of the m-th harmonic of capacitors' voltages by a monochromatic input and subsequent summation of these voltages at the output port. We also see that, theoretically, we could replace square switching functions with harmonic ones with appropriate frequencies and obtain a similar solution. The role of other harmonics in the response of the N-path filter is largely parasitic.

From (44) and (45), we can also obtain $h_{12,0}$ and $h_{22,0}$ by simply swapping p and q which yields

$$h_{12,0} \approx \frac{\operatorname{sinc}_{\pi}^{2}(r/N)}{2 + j\omega_{r}N\tau}e^{-jr\omega_{s}\Delta T},\tag{48}$$

$$h_{22,0} = h_{11,0} \approx \frac{\operatorname{sinc}_{\pi}^{2}(r/N)}{2 + j\omega_{r}N\tau}.$$
 (49)

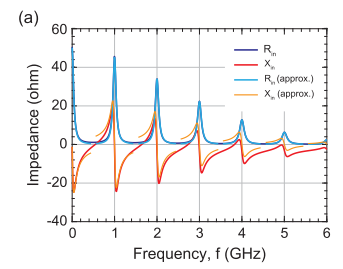
Finally, substituting (46)-(49) into (40) we obtain the following solution for the scattering matrix at the fundamental frequency:

$$\mathbf{S}_0 = \begin{bmatrix} S_{11,0} & S_{12,0} \\ S_{21,0} & S_{22,0} \end{bmatrix} = \begin{bmatrix} A - 1 & Ae^{-jr\omega_s \Delta T} \\ Ae^{jr\omega_s \Delta T} & A - 1 \end{bmatrix}, \quad (50)$$

with

$$A = \frac{\operatorname{sinc}_{\pi}^{2}(r/N)}{1 + j\frac{\omega_{r}N\tau}{2}}.$$
 (51)

To verify our solution, in Fig. 7 we plot the approximate scattering parameters based on Eq. (50) in the vicinity of transmission peaks at f = 0, f_s , $2f_s$, ... against a complete solution given by Eqs. (37), (39) and (40) for $\mathcal{R} = \{r\}$ and $\mathcal{N} = \{-60, \ldots, +60\} \setminus \mathcal{R}$ for $\Delta T = 3T_s/4$ and the rest of parameters being the same as in Fig. 4. Near the transmission peaks, the simplified solution indeed provides excellent agreement with the magnitudes and phases of the exact scattering parameters, enabling an effective design tool to optimize the overall response. Away from the peaks, the approximate solution predictably deviates, since the assumption of a single



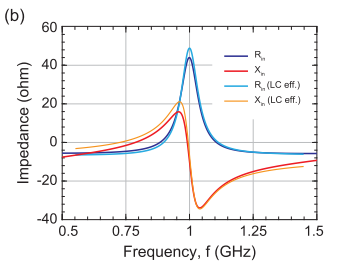


Fig. 8. (a) Real and imaginary parts of the input impedance $Z_{in} = R_{in} + j X_{in}$ of an N-path network with the same parameters as in Fig. 4 computed using full and approximate solutions. The network is connected to the input and output port through the same real and constant impedance $R_0 = 50$ ohm. (b) Input impedance of the same network at the vicinity of $f \approx f_s$ and the input impedance of an equivalent parallel LC tank with effective capacitance and inductance evaluated using Eqs. (58) and (59), respectively.

HTF being large does not hold anymore. From Eq. (50), we also see that $|S_{21,0}(f=kf_s)| \approx \mathrm{sinc}_{\pi}^2(k/N)$ with k being a positive integer. To illustrate this, in Fig. 7(a) we plot a function $\mathrm{sinc}_{\pi}^2(f/Nf_s)$ which bounds N-path filtering network transmission for any N and f_s . From Eq. (50), we can also easily find that the 3 dB bandwidth, Δf_{3dB} , computed from the top of each peak is

$$\Delta f_{\rm 3dB} \approx \frac{2\sqrt{3}}{\pi N \tau}.$$
 (52)

For the peak centered at f=1 GHz, we obtain $\Delta f_{\rm 3dB}=275.7$ MHz while the actual value is 280 MHz, a discrepancy of less than 3%. These results confirm and provide quantitative evidence that an increased number of paths narrows the bandwidth of each peak and enhances the amplitudes of transmission for higher frequencies.

A. Input Impedance

Using the analytic scattering matrix (50), we find the baseband impedance matrix [35] of the *N*-path filter:

$$\mathbf{Z} = R_0 \ B \begin{bmatrix} 1 & e^{-jr\omega_s \Delta T} \\ e^{jr\omega_s \Delta T} & 1 \end{bmatrix}, \tag{53}$$

with

$$B = \frac{1}{2} \frac{A}{1 - A}. (54)$$

Note that the expression above is derived under the assumption that the N-path network is connected to source and load ports through the same real impedance R_0 . Using (53) we can easily compute the baseband input impedance $Z_{in} = R_{in} + jX_{in}$ of the N-path filter connected to a load R_0 :

$$Z_{in} = Z_{11} - \frac{Z_{12}Z_{21}}{Z_{22} + R_0}$$

$$= R_0 \frac{\operatorname{sinc}_{\pi}^2(r/N)}{2 - \operatorname{sinc}_{\pi}^2(r/N) + j\omega_r N\tau}.$$
(55)

We note that Eq. (55) yields both real and imaginary parts of the input impedance. However, exactly at the transmission peaks k = 0, 1, 2, ... we have $\omega_r = 0$, leading to a purely real input impedance, as expected at resonance:

$$Z_{in,k} = R_0 \frac{\operatorname{sinc}_{\pi}^2(k/N)}{2 - \operatorname{sinc}_{\pi}^2(k/N)}.$$
 (56)

In Fig. 7(a), we compare the solution given by (55) in the vicinity of transmission peaks and the exact input impedance of the *N*-path network for the same combinations of parameters as in Fig. 4. It is seen that the real part of the analytic curves closely match the exact solution. The discrepancy far from the transmission peaks originates predominantly from the reactive part of the impedance. Most noticeably, the systematic offset of the exact reactance curves originates from the fact that we discarded all terms but one in summations (37) and (39).

B. Equivalent LC Circuit Model

It is known that for real source and load impedances, the behavior of an N-path filter in the vicinity of transmission peaks can be approximated by a parallel RLC circuit [27]. From (55) we obtain the input impedance in vicinity of the first peak (k = -r = 1):

$$Z \approx R_0 \frac{\operatorname{sinc}_{\pi}^2(1/N)}{1 + j\omega_{-1}N\tau},$$
 (57)

which yields the full-width half-maximum (FWHM) bandwidth $\Delta\omega=2/N\tau$. The bandwidth of a parallel LC circuit connected in parallel to the real load impedance R_0 is $\Delta\omega_{LC}=1/R_0C$, from which we immediately obtain the effective capacitance

$$C_{\text{eff}} = \frac{1}{2}NC,\tag{58}$$

where C is the single-branch capacitance of the N-path network. The effective inductance can be found from the LC resonance condition $\omega_0^2 = 1/LC$ by substituting $\omega_0 = \omega_s$:

$$L_{\rm eff} = \frac{2}{\omega_{\rm c}^2 NC}.$$
 (59)

In Fig. 7(b), we verify our findings by comparing the input impedance of the effective parallel LC circuit with the input impedance of the N-path network in the vicinity of the first transmission peak, and find a very good agreement. Eqs. (58) and (59) are also in agreement with the expressions derived in [27]. We once again stress that the N-path filter can be accurately modeled as a parallel LC circuit only when its source and load impedances are real and time-invariant.

VI. CONCLUSION

The perturbation approach presented in this article enabled us to develop an efficient and highly-accurate frequency-domain solution for *N*-path switched capacitive networks. We obtained excellent agreement between analytic results and circuit simulations for all combinations of parameters including less common scenarios, such as when clocks on each branch overlap, with significantly reduced computation time. Our technique compares favorably to the state-of-the-art state-space analysis by providing an equally accurate solution for harmonic transfer functions while being substantially easier to implement and analyze. The obtained solution remains accurate at all frequencies and converges rapidly with the increase in the number of harmonics included in the analysis. Thus, our method can be used as a reliable substitute or

verification of numerical results and as a useful tool for early-stage *N*-path network design, especially because it can easily handle networks with an arbitrary number of paths.

For the case when the *N*-path network is operated in the filtering regime, we obtained simple closed-form expressions for complex scattering parameters, impedance matrix and input impedance in the vicinity of transmission peaks, enabling simple and accurate extraction of key performance metrics such as insertion and return loss, bandwidth, etc.

Finally, our approach can be readily used to analyze *N*-path networks with arbitrary number of ports and can also be generalized to include the case of complex impedance blocks in each branch.

APPENDIX A

MATRIX INVERSION USING PERTURBATION THEORY

Perturbation theory states that for any system of equations $\mathbf{A} \cdot \mathbf{x}_0 = \mathbf{b}$, a small perturbation $\delta \mathbf{A}$ leads to a small perturbation $\delta \mathbf{x}$ of the solution vector \mathbf{x}_0 . The smallness of perturbation should be understood in the sense that it does not lead to a significant change in eigenvalues of the original matrix \mathbf{A} . Introducing a dimensionless parameter $0 < \varepsilon \ll 1$, we can write the perturbed system as

$$(\mathbf{A} + \varepsilon \delta \mathbf{A}) \cdot \mathbf{x} = \mathbf{b},\tag{60}$$

and present the new vector \mathbf{x} as a series in the power of ε as

$$\mathbf{x} = \varepsilon^0 \mathbf{x}_0 + \varepsilon^1 \mathbf{x}_1 + \varepsilon^2 \mathbf{x}_2 + \dots$$
 (61)

Substituting (61) into (60) and equating the terms with the same power of ε yields:

$$O(\varepsilon^{0}): \quad \mathbf{x}_{0} = \mathbf{A}^{-1} \cdot \mathbf{b},$$

$$O(\varepsilon^{1}): \quad \mathbf{x}_{1} = -\mathbf{A}^{-1} \cdot \delta \mathbf{A} \cdot \mathbf{x}_{0},$$

$$O(\varepsilon^{2}): \quad \mathbf{x}_{2} = -\mathbf{A}^{-1} \cdot \delta \mathbf{A} \cdot \mathbf{x}_{1},$$

$$\dots$$
(62)

Then by letting $\varepsilon = 1$ we obtain the following solution for **x** from Eq. (61):

$$\mathbf{x} = \mathbf{A}^{-1} \cdot \sum_{n=0}^{\infty} (-1)^n (\delta \mathbf{A} \cdot \mathbf{A}^{-1})^n \cdot \mathbf{b}.$$
 (63)

Finally, since $\mathbf{x} = (\mathbf{A} + \varepsilon \delta \mathbf{A})^{-1} \cdot \mathbf{b}$, we conclude that

$$(\mathbf{A} + \delta \mathbf{A})^{-1} = \mathbf{A}^{-1} \cdot \sum_{n=0}^{\infty} (-1)^n (\delta \mathbf{A} \cdot \mathbf{A}^{-1})^n.$$
 (64)

For sufficiently small perturbations, we can limit ourselves to only the first-order correction:

$$(\mathbf{A} + \delta \mathbf{A})^{-1} \approx \mathbf{A}^{-1} - \mathbf{A}^{-1} \cdot \delta \mathbf{A} \cdot \mathbf{A}^{-1}. \tag{65}$$

APPENDIX B

FLOQUET SCATTERING PARAMETERS

Scattering parameters of a linear time-invariant (LTI) system relate the amplitudes of incoming and outgoing power waves at all ports. Specifically, for an incoming power wave a_j at the port j and the outgoing power wave b_i at the port i the scattering parameter is defined as $S_{ij} = b_i/a_j$. Linearity of

the network enables us to use the superposition principle to obtain amplitudes of all outgoing power waves as a linear combination of all incoming power waves in a matrix form:

$$b_i = \sum_i S_{ij} a_j. (66)$$

If the network is modulated with periodicity $T_s = 2\pi/\omega_s$, Eq. (66) becomes time-varying:

$$b_i(t) = \sum_j S_{ij}(t)a_j(t). \tag{67}$$

Due to periodicity, we can present the scattering matrix elements $S_{ij}(t)$ as a Fourier series:

$$S_{ij}(t) = \sum_{n=-\infty}^{+\infty} S_{ij,n} e^{jn\omega_s t},$$
(68)

with

$$S_{ij,n} = \frac{1}{T_s} \int_{-T_s/2}^{T_s/2} S_{ij}(t) e^{-jn\omega_s t} dt.$$
 (69)

Periodically time-varying power waves $a_j(t)$ and $b_i(t)$ can be presented as Fourier-Floquet sums over an infinite set of discrete harmonics $\omega_m = \omega + m\omega_s$ with $m = 0, \pm 1, \pm 2, ...$:

$$\left\{ \begin{array}{l} a_j(t) \\ b_i(t) \end{array} \right\} = \sum_{m=-\infty}^{+\infty} \left\{ \begin{array}{l} a_{j,m} \\ b_{i,m} \end{array} \right\} e^{j\omega_m t}.
 \tag{70}$$

Substituting Eqs. (68) and (70) into (67) and equating the terms oscillating at similar frequencies, we obtain:

$$b_{i,m} = \sum_{j} \sum_{n = -\infty}^{\infty} S_{ij,m-n} a_{j,n},$$
 (71)

with $S_{ij,mn} \equiv S_{ij,m-n}$ being entries of a Floquet scattering matrix (FSM) relating the incoming and outgoing power waves oscillating at frequencies ω_m and ω_n . In a vector form, we can rewrite Eq. (71) as

$$\mathbf{b}_i = \sum_j \mathbf{S}_{ij} \cdot \mathbf{a}_j,\tag{72}$$

where

$$\mathbf{b}_{i} = \begin{pmatrix} \vdots \\ b_{i,-2} \\ b_{i,-1} \\ b_{i,0} \\ b_{i,1} \\ b_{i,2} \\ \vdots \end{pmatrix}, \quad \mathbf{a}_{j} = \begin{pmatrix} \vdots \\ a_{j,-2} \\ a_{j,-1} \\ a_{j,0} \\ a_{j,1} \\ a_{j,2} \\ \vdots \end{pmatrix}, \quad (73)$$

and

$$\mathbf{S}_{ij} = \begin{bmatrix} \ddots & & \vdots & & & \\ & S_{ij,0} & S_{ij,-1} & S_{ij,-2} & & & \\ \dots & S_{ij,1} & S_{ij,0} & S_{ij,-1} & \dots & & \\ & & S_{ij,2} & S_{ij,1} & S_{ij,0} & & & & \\ & & \vdots & & \ddots & & & \\ \end{bmatrix}.$$
(74)

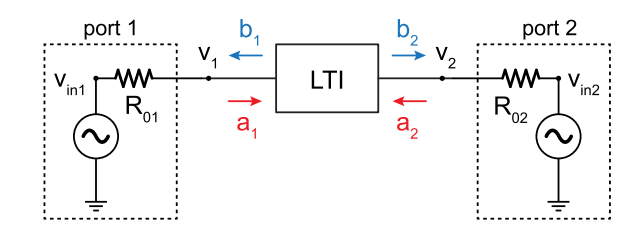


Fig. 9. Linear time-invariant (LTI) network connected to two ports with impedances R_{01} and R_{02} driven by source voltages $v_{\rm in1}$ and $v_{\rm in2}$, respectively. v_i with i=1,2 denote port voltages; a_i and b_i are amplitudes of power waves entering and exiting the network at each port.

APPENDIX C

RELATION BETWEEN FLOQUET SCATTERING PARAMETERS AND HARMONIC TRANSFER FUNCTIONS

To establish a relation between scattering parameters and harmonic transfer functions, consider a 2-port linear time-invariant system connected to the two voltage sources $v_{\text{in}1}$ and $v_{\text{in}2}$ through resistors R_{01} and R_{02} . First, let us assume $v_{\text{in}2} = 0$ in which case the voltages v_1 and v_2 can be found through transfer functions as h_{11} and h_{21} : $v_1 = h_{11}v_{\text{in}1}$, $v_2 = h_{21}v_{\text{in}1}$.

Amplitudes of power waves entering and exiting the ports (see Fig. 9) can be related to voltages v_i and currents i_i as [36]:

$$a_i = \frac{1}{2\sqrt{R_{0i}}}(v_i + R_{0i}i_i),\tag{75}$$

$$b_i = \frac{1}{2\sqrt{R_{0i}}}(v_i - R_{0i}i_i). \tag{76}$$

Applying the KVL, it is easy to see that:

$$a_1 = \frac{1}{2\sqrt{R_{01}}}v_{\text{in}1},\tag{77}$$

$$b_1 = \frac{1}{2\sqrt{R_{01}}}(2v_1 - v_{\text{in}1}) = \frac{2h_{11} - 1}{2\sqrt{R_{01}}}v_{\text{in}1}, \tag{78}$$

$$a_2 = \frac{1}{2\sqrt{R_{02}}}(v_2 - v_2) = 0, (79)$$

$$b_2 = \frac{1}{2\sqrt{R_{02}}}(v_2 + v_2) = \frac{h_{21}}{\sqrt{R_{02}}}v_{\text{in1}}, \tag{80}$$

from where

$$S_{11} = b_1/a_1 = 2h_{11} - 1,$$
 (81)

$$S_{21} = b_2/a_1 = 2\sqrt{\frac{R_{01}}{R_{02}}}h_{21}. (82)$$

Following the same procedure for the case $v_{in1} = 0$, we can similarly obtain

$$S_{12} = b_1/a_2 = 2\sqrt{\frac{R_{02}}{R_{01}}}h_{12},$$
 (83)

$$S_{22} = b_2/a_2 = 2h_{22} - 1.$$
 (84)

Finally, we can leverage the linearity of the network to combine Eqs. (81), (82) with (83), (84):

$$b_i = \sum_j S_{ij} a_j, \tag{85}$$

where

$$S_{ij} = 2\sqrt{\frac{R_{0j}}{R_{0i}}}h_{ij} - \delta_{ij}.$$
 (86)

If the LTI block is replaced by a linear time-periodic (LTP) network, we can follow the same procedure by treating each harmonic at every physical port as an independent port enabling us to establish a relation between Floquet scattering parameters $S_{ij,mn}$ defined in Appendix B and harmonic transfer functions $h_{ii,mn}$:

$$S_{ij,mn} = 2\sqrt{\frac{R_{0j}}{R_{0i}}}h_{ij,mn} - \delta_{ij}\delta_{mn}.$$
 (87)

where i, j and m, n are port and harmonic numbers, respectively. Note that Eq. (87) holds only for the case when the impedance R_{0i} of all ports is real and constant. If this is not the case, a more general expression can be obtained which we omit here for the sake of brevity.

Finally, in case when all ports have the same impedance R_0 , Eq. (87) reduces to

$$S_{ij,mn} = 2h_{ij,mn} - \delta_{ij}\delta_{mn}.$$
 (88)

REFERENCES

- H. Busignies and M. Dishal, "Some relations between speed of indication, bandwidth, and signal-to-random-noise ratio in radio navigation and direction finding," *Proc. IRE*, vol. 37, no. 5, pp. 478–488, May 1949.
- [2] B. D. Smith, "Analysis of commutated networks," Trans. IRE Prof. Group Aeronaut. Navigational Electron., vol. 10, pp. 21–26, Dec. 1953.
- [3] W. R. Lepage, C. R. Cahn, and J. S. Brown, "Analysis of a comb filter using synchronously commutated capacitors," *Trans. Amer. Inst. Electr. Eng., Part I, Commun. Electron.*, vol. 72, no. 1, pp. 63–68, Mar. 1953.
- [4] E. A. M. Klumperink, H. J. Westerveld, and B. Nauta, "N-path filters and mixer-first receivers: A review," in *Proc. IEEE Custom Integr. Circuits Conf. (CICC)*, Apr. 2017, pp. 1–8.
- [5] M. Tymchenko, D. Sounas, A. Nagulu, H. Krishnaswamy, and A. Alù, "Quasi-electrostatic wave propagation beyond the delay-bandwidth limit in switched networks," *Phys. Rev. X*, vol. 9, no. 3, Jul. 2019, Art. no. 031015.
- [6] A. Nagulu, M. Tymchenko, A. Alu, and H. Krishnaswamy, "Ultra compact, ultra wideband, DC-1 GHz CMOS circulator based on quasi-electrostatic wave propagation in commutated switched capacitor networks," in *Proc. IEEE Radio Freq. Integr. Circuits Symp. (RFIC)*, Los Angeles, CA, USA, Aug. 2020, pp. 55–58.
- [7] E. Everett, A. Sahai, and A. Sabharwal, "Passive self-interference suppression for full-duplex infrastructure nodes," *IEEE Trans. Wireless Commun.*, vol. 13, no. 2, pp. 680–694, Feb. 2014.
- [8] A. Nagulu, A. Gaonkar, S. Ahasan, T. Chen, G. Zussman, and H. Krishnaswamy, "A full-duplex receiver leveraging multiphase switched-capacitor-delay based multi-domain FIR filter cancelers," in Proc. IEEE Radio Freq. Integr. Circuits Symp. (RFIC), Los Angeles, CA, USA, Aug. 2020, pp. 43–46.
- [9] J. Roderick, H. Krishnaswamy, K. Newton, and H. Hashemi, "Silicon-based ultra-wideband beam-forming," *IEEE J. Solid-State Circuits*, vol. 41, no. 8, pp. 1726–1739, Aug. 2006.
- [10] C. Thakkar, N. Narevsky, C. D. Hull, and E. Alon, "Design techniques for a mixed-signal I/Q 32-coefficient R-feedforward equalizer, 100coefficient decision feedback equalizer in an 8 Gb/s 60 GHz 65 nm LP CMOS receiver," *IEEE J. Solid-State Circuits*, vol. 49, no. 11, pp. 2588–2607, Nov. 2014.
- [11] N. Reiskarimian and H. Krishnaswamy, "Magnetic-free nonreciprocity based on staggered commutation," *Nature Commun.*, vol. 7, Apr. 2016, Art. no. 11217.
- [12] L. E. Franks and I. W. Sandberg, "An alternative approach to the realization of network transfer functions: Then-path filter," *Bell Syst. Tech. J.*, vol. 39, no. 5, pp. 1321–1350, Sep. 1960.

- [13] T. Iizuka and A. A. Abidi, "FET-R-C circuits: A unified treatment— Part I: Signal transfer characteristics of a single-path," *IEEE Trans. Circuits Syst. I, Reg. Papers*, vol. 63, no. 9, pp. 1325–1336, Sep. 2016.
- [14] T. Iizuka and A. A. Abidi, "FET-R-C circuits: A unified treatment— Part II: Extension to multi-paths, noise figure, driving-point impedance," *IEEE Trans. Circuits Syst. I, Reg. Papers*, vol. 63, no. 9, pp. 1337–1348, Sep. 2016.
- [15] A. Mirzaei, H. Darabi, and D. Murphy, "Architectural evolution of integrated M-phase high-Q bandpass filters," *IEEE Trans. Circuits Syst. I*, *Reg. Papers*, vol. 59, no. 1, pp. 52–65, Jan. 2012.
- [16] D. Yang, C. Andrews, and A. Molnar, "Optimized design of N-phase passive mixer-first receivers in wideband operation," *IEEE Trans. Circuits Syst. I, Reg. Papers*, vol. 62, no. 11, pp. 2759–2770, Nov. 2015.
- [17] S. Hameed, M. Rachid, B. Daneshrad, and S. Pamarti, "Frequency-domain analysis of N-path filters using conversion matrices," IEEE Trans. Circuits Syst. II, Exp. Briefs, vol. 63, no. 1, pp. 74–78, Jan. 2016.
- [18] P. P. Vaidyanathan and S. K. Mitra, "Polyphase networks, block digital filtering, LPTV systems, and alias-free QMF banks: A unified approach based on pseudocirculants," *IEEE Trans. Acoust., Speech, Signal Process.*, vol. 36, no. 3, pp. 381–391, Mar. 1988.
- [19] L. Toth and E. Simonyi, "A new approach for the Z-domain analysis of linear periodically time-varying discrete time systems," in *Proc. IEEE Int. Symp. Circuits Syst.*, New Orleans, LA, USA, May 1990, pp. 1185–1188.
- [20] S. Pavan and E. Klumperink, "Simplified unified analysis of switched-RC passive mixers, samplers, and N-path filters using the adjoint network," *IEEE Trans. Circuits Syst. I, Reg. Papers*, vol. 64, no. 10, pp. 2714–2725, Oct. 2017.
- [21] S. Pavan and E. Klumperink, "Generalized analysis of high-order switch-RC N-path mixers/filters using the adjoint network," *IEEE Trans. Circuits Syst. I, Reg. Papers*, vol. 65, no. 10, pp. 3267–3278, Oct. 2018.
- [22] C. Scarborough and A. Grbic, "Accelerated N-path network analysis using the Floquet scattering matrix method," *IEEE Trans. Microw. Theory Techn.*, vol. 68, no. 4, pp. 1248–1259, Apr. 2020.
- [23] T. Strom and S. Signell, "Analysis of periodically switched linear circuits," *IEEE Trans. Circuits Syst.*, vol. 24, no. 10, pp. 531–541, Oct 1977
- [24] M. C. M. Soer, E. A. M. Klumperink, P. T. de Boer, F. E. van Vliet, and B. Nauta, "Unified frequency-domain analysis of switched-series-RC passive mixers and samplers," *IEEE Trans. Circuits Syst. I, Reg. Papers*, vol. 57, no. 10, pp. 2618–2631, Oct. 2010.
- [25] A. Ghaffari, E. A. M. Klumperink, M. C. M. Soer, and B. Nauta, "Tunable high-Q N-path band-pass filters: Modeling and verification," *IEEE J. Solid-State Circuits*, vol. 46, no. 5, pp. 998–1010, May 2011.
- [26] N. Reiskarimian, J. Zhou, T.-H. Chuang, and H. Krishnaswamy, "Analysis and design of two-port N-path bandpass filters with embedded phase shifting," *IEEE Trans. Circuits Syst. II, Exp. Briefs*, vol. 63, no. 8, pp. 728–732, Aug. 2016.
- [27] N. Reiskarimian and H. Krishnaswamy, "Design of all-passive higher-order CMOS N-path filters," in *Proc. IEEE Radio Freq. Integr. Circuits Symp. (RFIC)*, May 2015, pp. 83–86.
- [28] M. Tavassoli and A. Jalali, "Analysis of an enhanced-Q N-path filter with improved even-order harmonic rejection," *Circuits, Syst., Signal Process.*, vol. 37, no. 3, pp. 939–964, Mar. 2018.
- [29] S. Pavan and E. Klumperink, "Analysis of the effect of source capacitance and inductance on *N*-path mixers and filters," *IEEE Trans. Circuits Syst. I, Reg. Papers*, vol. 65, no. 5, pp. 1469–1480, May 2018.
- [30] L. N. Trefethen and D. Bau, Numerical Linear Algebra Philadelphia, PA, USA: Society Industrial Applied Mathematics, 1997.
- [31] A. V. Kats, P. D. Pavitskii, and I. S. Spevak, "Theory of resonant diffraction in periodic impedance structures," *JETP*, vol. 78, p. 42, Jan. 1994.
- [32] G. Kron, Tensor Analysis of Networks. Hoboken, NJ, USA: Wiley, 1939.
- [33] PSS Solver, Cadence SpectreRF. Accessed: 2020. [Online]. Available: https://www.cadence.com/
- [34] Python Implementation of the Present N-Path Network Analysis. Accessed: 2020. [Online]. Available: https://github.com/mtymchenko/npaths
- [35] D. A. Frickey, "Conversions between S, Z, Y, H, ABCD, and T parameters which are valid for complex source and load impedances," *IEEE Trans. Microw. Theory Techn.*, vol. 42, no. 2, pp. 205–211, Feb. 1994
- [36] K. Kurokawa, "Power waves and the scattering matrix," IEEE Trans. Microw. Theory Techn., vol. 13, no. 2, pp. 194–202, Mar. 1965.



Mykhailo Tymchenko received the B.S. and M.S. degrees in theoretical physics from V. N. Karazin Kharkiv National University, Kharkiv, Ukraine, in 2009 and 2010, respectively, and the Ph.D. degree in electrical engineering from The University of Texas at Austin, Austin, TX, USA, in 2019.

From 2010 to 2013, he was a Junior Research Scientist with the Usikov Institute of Radiophysics and Electronics, Kharkiv. He was a Visiting Scholar with the University of Zaragoza, Zaragoza, Spain, in 2012 and 2013. In 2018, he was an Intern with the

Emerging Materials, Components and Devices Laboratory, Nokia Bell Labs, Murray Hill, NJ, USA. In 2019, he joined as a Technical Staff at Lightmatter, Boston, MA, USA. He has authored or coauthored more than 25 articles in top-tier scientific journals and one book chapter. He holds two patents. His current research interests include time-periodic systems and circuits, integrated photonics, linear and nonlinear metasurfaces, plasmonics, and topological photonics. He was a recipient of The University of Texas Graduate School Fellowship from 2013 to 2017 and the Student Paper Competition Finalist at the 10th International Congress on Advanced Electromagnetic Materials in Microwaves and Optics in 2016 (Second Place).



Aravind Nagulu (Member, IEEE) received the B.Tech. and M.Tech. degrees in electrical engineering from IIT Madras, Chennai, India, in 2016. He is currently pursuing the Ph.D. degree in electrical engineering with Columbia University, New York, NY, USA.

During his master's studies, he was involved in the implementation of a high-resolution continuous time delta-sigma modulator. His current research interests include exploring new directions to achieve fully integrated, magnetless non-reciprocity, and to

provide experimental validation for non-reciprocal components catering to a wide range of applications ranging from RF/mmWave communication, frequency-modulated continuous-wave (FMCW) radars, and quantum information processing.

Mr. Nagulu was a recipient of the IEEE RFIC Symposium Best Student Paper Award (First Place) in 2018, the IEEE Solid-State Circuits Society Predoctoral Achievement Award, the ISSCC Analog Devices Outstanding Student Designer Award, the IEEE MTT-S Graduate Fellowship in 2019, and the IEEE RFIC Symposium Best Student Paper Finalist in 2020.



Harish Krishnaswamy (Senior Member, IEEE) received the B.Tech. degree in electrical engineering from IIT Madras, Chennai, India, in 2001, and the M.S. and Ph.D. degrees in electrical engineering from the University of Southern California (USC), Los Angeles, CA, USA, in 2003 and 2009, respectively.

In 2009, he joined the Department of Electrical Engineering, Columbia University, New York, NY, USA, where he is currently an Associate Professor and the Director of the Columbia High-Speed and

Millimeter-Wave IC Laboratory (CoSMIC). In 2017, he co-founded Mix-Comm Inc., a venture-backed startup, to commercialize CoSMIC Laboratory's advanced wireless research. His current research interests include integrated devices, circuits, and systems for a variety of RF, mm-wave, and sub-mm-wave applications. He has been a member of the Technical Program Committee of several conferences, including the IEEE International Solid-State Circuits Conference since 2015 and the IEEE Radio Frequency Integrated Circuits Symposium since 2013. He was a recipient of the IEEE International Solid-State Circuits Conference Lewis Winner Award for Outstanding Paper in 2007, the Best Thesis in Experimental Research Award from the USC Viterbi School of Engineering in 2009, the Defense Advanced Research Projects Agency Young Faculty Award in 2011, the 2014 IBM Faculty Award, the Best Demo Award at the 2017 IEEE ISSCC, and the Best Student Paper Awards at the 2015, 2018, and 2020 IEEE Radio Frequency Integrated Circuits Symposium. He currently serves as a Distinguished Lecturer for the IEEE Solid-State Circuits Society and a member for the DARPA Microelectronics Exploratory Council.



Andrea Alù (Fellow, IEEE) received the Laurea, M.S., and Ph.D. degrees from the University of Roma Tre, Rome, Italy, in 2001, 2003, and 2007, respectively. He is currently the Founding Director of the Photonics Initiative with the CUNY Advanced Science Research Center. He is also the Einstein Professor of Physics with the CUNY Graduate Center, a Professor of electrical engineering with the City College of New York, and an Adjunct Professor and a Senior Research Scientist with The University of Texas at Austin. After spending one year as a

Post-Doctoral Research Fellow at UPenn in 2009, he joined the Faculty of The University of Texas at Austin, where he was the Temple Foundation Endowed Professor until 2018. His current research interests include metamaterials and plasmonics, electromagnetics, optics and nanophotonics, acoustics, scattering, nanocircuits and nanostructures, miniaturized antennas and nanoantennas, and RF antennas and circuits. He is a fellow of the National Academy of Inventors, AAAS, OSA, APS, and SPIE, a Highly Cited Researcher since 2017, a five times Blavatnik Awardee, a Simons Investigator in Physics, the IEEE Antennas and Propagation Society Distinguished Lecturer, and a OSA Traveling Lecturer. He has received several awards for his scientific work, including the URSI Issac Koga Gold Medal in 2011, the OSA Adolph Lomb Medal in 2013, the NSF Alan T. Waterman Award in 2015, the ICO Prize in Optics in 2016, the Vannevar Bush Faculty Fellowship from DoD in 2019, and the IEEE Kiyo Tomiyasu Award in 2020.